IECON 2021 - 47th Annual Conference of the IEEE Industrial Electronics Society | 978-1-6654-3554-3/21/$31.00 ©2021 IEEE | DOI: 10.1109/IECON48115.2021.9589692

Mission Profile-Oriented Active Thermal Control of a Bidirectional Three-Level Buck-Boost GaN-Based DC-DC Converter for Electric Vehicles Powertrains

Christian A. Rojas, Ruben Gonzalez
Department of Electronic Engineering
Universidad Tecnica Federico Santa Maria
Valparaiso, Chile
c.a.rojas@ieee.org

Leonardo Callegaro
School of Engineering
Macquarie University
Sydney, NSW, Australia
leonardo.callegaro@mq.edu.au

Hector Young
Department of Electrical Engineering
Universidad de La Frontera
Temuco, Chile
hector.young@ufrontera.cl

***Abstract*—One of current challenges in high-density electric vehicles (EVs) is the efficient thermal control of power converters and the reliable management of power flows in motoring/breaking mode for the battery bank. In this line, this paper presents an Active Thermal Control (ATC) scheme to regulate thermal stress in Gallium Nitride High Electron Mobility Transistors (GaN HEMTs) devices of a three-level bidirectional buck-boost DC-DC converter (TLBBC) as a power interface between battery and motor inverter. The TLBBC is designed to operate at a rated power of 20 kW as part of a modular system, by using parallel GaN devices. Proposed control schemes are implemented using systematic linear control design. Finally, the system is simulated and tested for a Mission Profile-Oriented (MPO) based on Highway Fuel Economy Test (HWFET) in order to validate the proposed control schemes.**

***Index Terms*—Active Thermal Control (ATC), DC-DC converter, Gallium Nitride (GaN), Highway Fuel Economy Test (HWFET), Mission Profile-Oriented (MPO), Three-level buck-boost converter (TLBBC), Voltage Balance Control (VBC).**

I. Introduction

TODAY, the need to use sustainable and clean energy is imperative and utilization of electric transport is a clear example to achieve this fundamental objective. In fact, this is reflected by an increased number of electric vehicles (EVs) within the automotive fleet worldwide [1]. High-density power converters solve the new challenges given by these new technologies, such as power-building-block design of high-power chargers and efficient powertrains [2], [3].

A powertrain consists of a battery pack as the energy storage system (ESS), bidirectional DC-DC and DC-AC converters and an electric motor, as shown in Fig. 1a. The bi-directional DC-DC converter is used to manage power flows between the battery and the inverter dc-link. This converter boosts the battery voltage up to the inverter dc-link voltage in the motor driving mode, and steps down the dc-link voltage to charge the battery in the regenerative deceleration and braking modes.

Many topologies can be used to build the DC-DC converter, which are able to manage bidirectional power flow between the battery and the inverter, such as Interleaved boost, three-level flying capacitor boost and three-level boost [4]. In fact, the three-level buck-boost DC-DC converter (TLBBC) as shown in Fig. 1c has been receiving good attention, because it has lower voltage stress in the semiconductors compared to two-level topologies, uses fewer switches compared to others three-level topologies [5], and is capable of operating at wide output voltage ranges [6], [7]. Furthermore, the stacked connection is possible in boost-buck [8] and buck-boost [9] modes.

Recently developed Gallium Nitride High Electron Mobility Transistors (GaN HEMTs) are being applied in many high-power converters because of their advantages, such as close to zero turn-off losses and higher power density compared to traditional Si MOSFETs [10]. One limitation of GaN devices is their lower breakdown voltage, although it is currently increasing from 650 to 1200 V [11], [12]. Power level limitations can be solved using stacked and serial-parallel design (Fig. 1b), which allows achieving higher power levels [13].

Conventional control objectives for bidirectional TLBBC are dc-link voltage regulation (VC) [14] and inner capacitor voltage balancing (VBC) [15]. Furthermore, battery current control (CC) is required during regeneration. Thermal stress is another critical control objective for GaN-based DC-DC

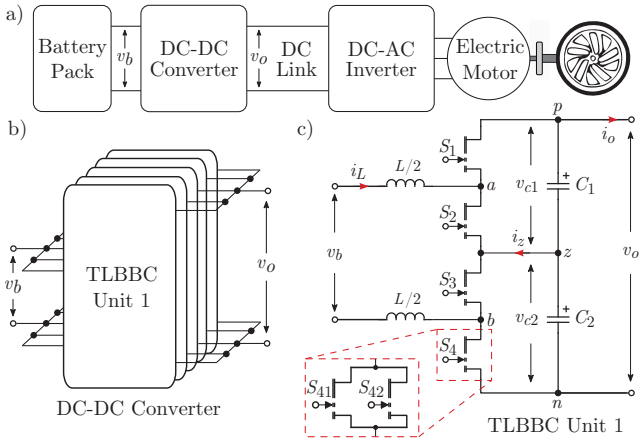

Fig. 1: Electric vehicle powertrain: a) general architecture b) parallel connection of n modules and c) one TLBBC module.

converters, since it affects strongly their lifetime [16], [17]. An adequate thermal model is also relevant to implement an effective temperature regulation, such as in [18], [19].

The active thermal control (ATC) is mainly implemented by changing the gate resistance, the PWM pulse pattern and the switching frequency [20]. In [21], an ATC strategy based on varying the converter switching frequency to regulate the operating temperature has been proposed. However, this method is validated just for motoring mode under boosting regime for piecewise constant power. In this paper, the ATC strategy proposed in [21] is extended to the buck regime, i.e., to the regenerative mode. The ATC strategy for boost and buck regimes is then validated using a Mission Profile-Oriented (MPO) scenario based on Highway Fuel Economy Test (HWFET) [22] and a realistic powertrain model, in order to validate the proposed control scheme.

This paper is organized as follows. Section II presents a summary of electrical, thermal and electro-mechanical modelling of the powertrain under study. Section III presents the overall control scheme. Section IV shows simulation results. Conclusion and future work are presented in Section V.

II. System Modelling

A. Operation Principle of TLBBC

The modelling of the TLBBC is performed for one unit of Fig. 1b. The TLBBC topology consists of four switches $\{S_1S_2S_3S_4\}$, an input filter composed of a pole-distributed inductor L and an output filter made of two capacitors C_1 and C_2. Each switch represents two GaN HEMT parallel-connected devices in order to achieve a higher-power level [13], [23]. In the motoring (boost) mode, the duty cycle of S_2 and S_3 is controlled, while S_1 and S_4 are switched complimentarily to S_2 and S_3, respectively. In the regenerative (buck) mode, the duty cycle of S_1 and S_4 is controlled, with S_2 and S_3 switched complimentarily to S_1 and S_4, respectively. Firing-pulse signals are commanded by phase-shift pulse width modulation (PS-PWM). Average modulation signals are represented by two duty cycles, d_2 to control S_1 and S_2, and d_3 to control S_3 and S_4. The TLBBC average model considers an operation in continuous conduction mode (CCM). Output voltage $v_o = v_{c1} + v_{c2}$ is assumed to be constant during the entire switching cycle.

B. DC-DC Converter Model

Duty cycles d_2 and d_3 are the control inputs, the switching cycle averaged state equations for Fig. 1c are

$$L\dot{i}_b = v_b - (1-d_2)v_{c1} - (1-d_3)v_{c2} \quad (1)$$

$$C_1\dot{v}_{c1} = (1-d_2)i_L - i_o \quad (2)$$

$$C_2\dot{v}_{c2} = (1-d_3)i_L - i_o \quad (3)$$

where the inductor current i_L and capacitor voltages v_{c1} and v_{c2} are the state variables. The input voltage v_b and output current i_o are assumed to be constant piecewise perturbations. A small-signal linearization of (1)-(3) around an operating point

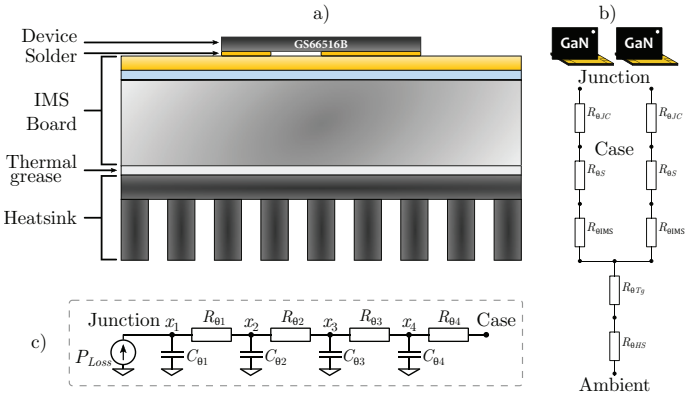

Fig. 2: Thermal model: a) IMS board; themal model between junction to b) ambient and to c) case.

with $\{V_{c1}{=}V_{c2}{=}V_c{=}V_o/2, I_L, D_2{=}D_3{=}D\}$ with $C_1{=}C_2{=}C$ and $\Delta\tilde{v}_c{=}\tilde{v}_{c1} - \tilde{v}_{c2}$, is given by:

$$\begin{bmatrix} \tilde{i}_L \\ \Delta\tilde{v}_c \\ \tilde{v}_o \end{bmatrix} \approx \begin{bmatrix} \frac{V_c}{Ls} & \frac{V_c}{Ls} \\ -\frac{I_L}{Cs} & \frac{I_L}{Cs} \\ \frac{2(1-D)V_c}{LCs^2} & \frac{2(1-D)V_c}{LCs^2} \end{bmatrix} \begin{bmatrix} \tilde{d}_2 \\ \tilde{d}_3 \end{bmatrix}. \quad (4)$$

This representation is useful to identify first order transfer functions to adjust each PI controller parameters. Major details about this model and its controller design are provided in [21].

C. Thermal Model

Thermal model considers that GaN devices are connected through an Insulated Metal Substrate (IMS) board to the heatsink [24] board with homogeneous behavior detailed in Fig. 2a. Proposed thermal model are based on a Cauer-type RC network and shown in Fig. 2b. P_{Loss} represents power losses of GaN device presented in Fig. 2c, which consist of conduction and switching losses. The junction temperature T_j estimation considers as input P_{Loss} and case temperature T_c,

$$T_j = P_{loss}R_{\theta jc} + T_c \quad (5)$$

$$P_{loss} = \frac{V_{DS}I_{DS}}{2}(t_{cr} + t_{vf} + t_{vr} + t_{cf})f_{sw} + I_{DS}^2R_{on} \quad (6)$$

where $R_{\theta jc}$ is the homogeneous thermal resistor between junction and case, V_{DS} and I_{DS} are the drain-source variables, R_{on} is the resistor during ON operation, $\{t_{cr}, t_{cf}\}$ and $\{t_{vr}, t_{vf}\}$ are the times during one ON and OFF cycle of current and voltage, respectively. Then, the junction temperature can be modified by changing the switching frequency

TABLE I: Thermal model parameters

Junction to case			Case to ambient		
Node x	$R_{\theta x}$ $^\circ C/W$	$C_{\theta x}$ $Ws/^\circ C$	Node y	$R_{\theta y}$ $^\circ C/W$	$C_{\theta y}$ $Ws/^\circ C$
1 GaN	0.006	$9.03{\cdot}10^{-5}$	S	0.2	0.01
2 Si	0.125	0.00629	IMS	0.7	0.01
3 Attachment	0.126	0.00141	Tg	0.2	0.01
4 Cu base	0.013	0.00214	HS	0.5	0.01

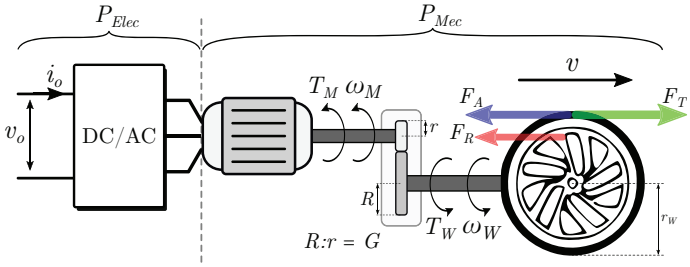

Fig. 3: Electromechanical powertrain model.

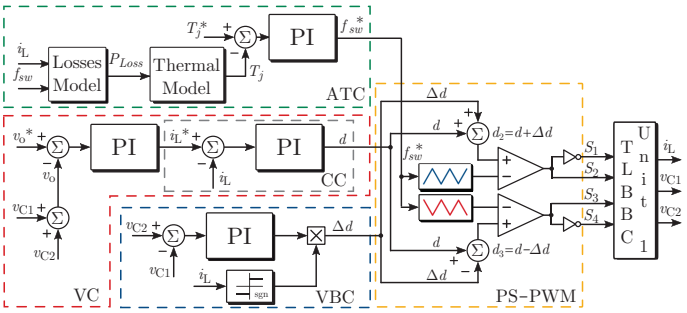

Fig. 4: Proposed control strategy.

f_{sw}. In this work, P_{Loss} is obtained through simulation with a provided power loss model by GaN Systems [25] [21].

Otherwise, to avoid a complex mathematical analysis to obtain an expression for a complete thermal model of the system, fitting a first-order model as (7), based on a simulation step response is an adequate approximation and sufficient to achieve accurate homogeneous thermal behavior.

$$G_{T_j f_{sw}} = \frac{T_j}{f_{sw}} = \frac{K_{th}}{\tau_{th} s + 1} \tag{7}$$

Considering the parameters shown in Table I [23], the parameters $K_{th} = 8.16 \cdot 10^{-4}$ °C·s and $\tau_{th} = 0.16535$ s for first-order thermal model have been obtained. Finally, thermal dynamics are assumed to be much slower than electrical dynamics.

D. Electromechanical Model

A simplified Electromechanical model is derived to obtain the required electric power given a driving mission profile. In this model, three main forces are considered: aerodynamic drag (F_A), friction (F_R) and traction (F_T) forces,

$$F_A + F_R = \frac{1}{2}\rho_\alpha c_d A v^2 + \mu_r (m_{EV} + m_p) g \tag{8}$$

$$F_T = (m_{EV} + m_p)\alpha + F_A + F_R \tag{9}$$

where α is the required acceleration, g=9.8m/s^2 and the parameter set $\{\rho_\alpha, c_d, A, m_{EV}, m_p\}$ is defined in Table II. Now, considering an ideal scenario where gearbox is modeled as a gain G, inverter and motor losses are neglected by simplicity, the mechanical power can be related to the electric torque T_M and wheels torque T_W,

$$P_{mec} = T_M \omega_M = T_W \omega_W \tag{10}$$

$$r\omega_M = R\omega_W \Rightarrow \frac{\omega_W}{\omega_M} = \frac{r}{R} = \frac{1}{G} \tag{11}$$

$$T_W = r_W F_T \Rightarrow T_M = \frac{r_W}{G} F_T \tag{12}$$

TABLE II: Electromechanical model parameters

Vehicle parameters		Driving parameters	
Parameter	Value	Parameter	Value
Vehicle mass, m_{EV}	1354 kg	Driver mass, m_p	100 kg
Wheel radius, r_W	0.292 m	Friction coeff., μ_r	0.02
Gearbox gain, G	9.665	Air density, ρ_α	1.225 kg/m^3
Frontal area, A	2.37 m^2	Traction coeff., c_d	0.29

where, the r_W is the wheel radius. Thus, the EV car and wheels speed are related as following

$$v = r_W \omega_W \tag{13}$$

and finally the electric power can be derived such as

$$P_{elec} = F_T v \tag{14}$$

where F_T is computed by considering parameters in Table II for a BMW i3 of 120 Ah EV model and the speed driving profile v is obtained from a HWFET standard test [22].

III. System Control

The overall proposed control scheme is shown in Fig. 4, and its objectives are to control the inductor current, the battery voltage and the junction temperature, and to balance the split capacitors voltage.

A. Converter Control

The transfer function between duty cycle and inductor current is derived from (4), where the expression is identical for both $\tilde{d}_2$ and $\tilde{d}_3$. This allows to employ a single current controller to obtain signal d, which contributes directly on d_2 and d_3, as shown in Fig. 4. On the other hand, the sign of transfer functions between duty cycles and capacitors voltage difference in (4) changes according with the operation mode due to sign of I_L. This controller generates signal Δd, which contributes positively on d_2, and in a negative way on d_3, as shown in Fig. 4. Finally, output voltage control is implemented by using a cascade control scheme to define a value of current reference as shown in Fig. 4 [26]. Because the expression in (4) is identical for $\tilde{d}_2$ and $\tilde{d}_3$, just one controller to obtain reference value for i_L is implemented. Systematic derivation of plants and controller design are provided in [21].

TABLE III: Simulation parameters

Components		Operating point	
Parameter	Value	Parameter	Value
L	2 mH	V_b	400 V
C_b	600 μF	I_b	50 A
C_1	330 μF	V_c	400 V
C_2	330 μF	V_o	800 V
S_1, S_2, S_3, S_4	2xGS66516B	D	0.5

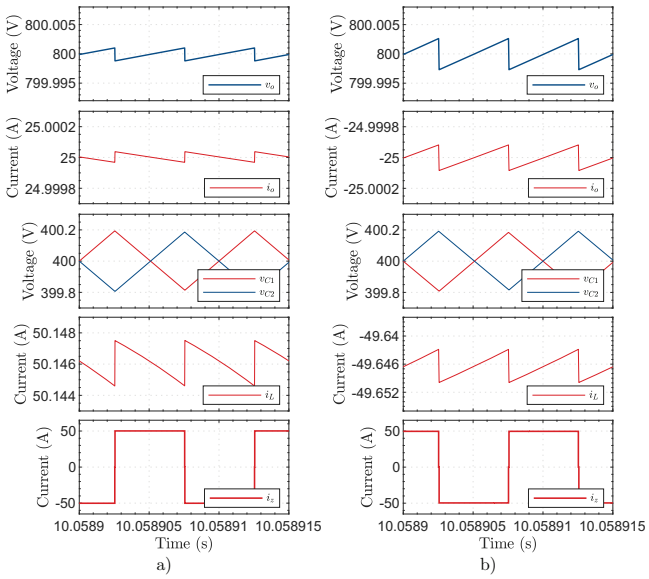

Fig. 5: Main variables: output voltage, output current, capacitor voltages, battery current and neutral point current under rated power for: a) boost and b) buck operation mode.

B. Active Thermal Control (ATC)

Thermal control is proposed to regulate the junction temperature T_j of each switches. Furthermore, due to the symmetrical operation between inner and external devices, a natural thermal balance between them is expected. In fact, during boost and buck mode $\{S_2, S_3\}$ and $\{S_1, S_4\}$ are mostly active, respectively. Then, it is required to identify the maximum temperature of switches,

$$T_j = \max\{T_{jS1}, T_{jS2}, T_{jS3}, T_{jS4}\} \tag{15}$$

Furthermore, junction temperature has a nonlinear behaviour when varying output power at fixed switching frequency, and has a linear behaviour when varying switching frequency at fixed output power [21]. For that reason, the junction temperature is regulated by varying the switching frequency. The switching frequency range used in this work is 50 to 500 kHz. The overall control scheme with the ATC loop for boost and buck mode are presented in Fig. 4.

IV. Simulation Results

The system is simulated in PLECS using a sampling rate of 20 kHz and by including GaN thermal models [25]. For validation, a 20 kW converter is designed considering the parameters shown in Table III, and implementing two parallel GS66516B [11] GaN HEMT for each switch. The battery pack capacity is 120Ah [27] modeled with an zero-order Thevenin model. Bandwidths for PI control loops CC, VC, VBC and ATC are 1 kHz, 100 Hz, 100 Hz and 25 Hz, respectively [21]. To verify the proposed control scheme, simulation results are presented for bidirectional operation modes under constant piecewise power profile and for a driving standard profile.

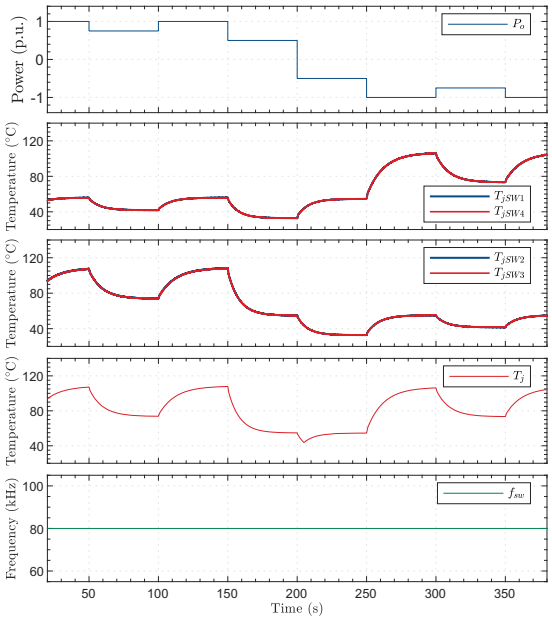

Fig. 6: Thermal behavior from boost to buck mode without ATC: output power P_o dictated by the chosen driving profile, estimated junction temperature of $\{S_1, S_4\}$, estimated junction temperature of $\{S_2, S_3\}$, maximum estimated junction temperature and applied switching frequency.

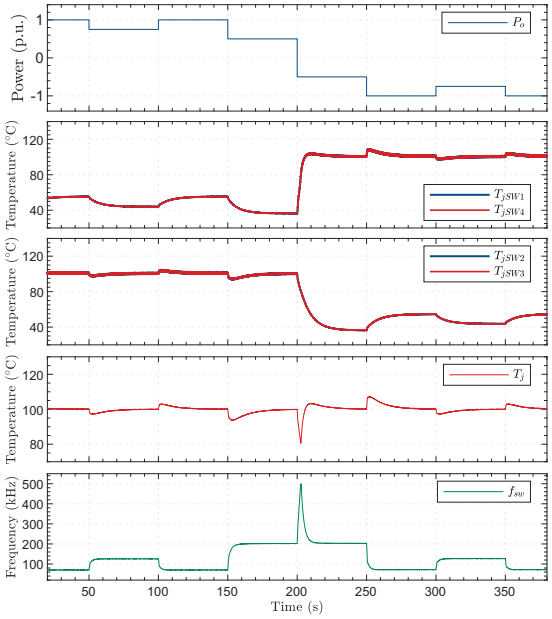

Fig. 7: Thermal behavior from boost to buck mode with ATC: output power, estimated junction temperature of $\{S_1, S_4\}$, estimated junction temperature of $\{S_2, S_3\}$, maximum estimated junction temperature and applied switching frequency.

A. Constant Piecewise Power Profile

The first test presents the bidirectional operation of the converter in Fig. 5 under rated conditions and ATC is disabled.

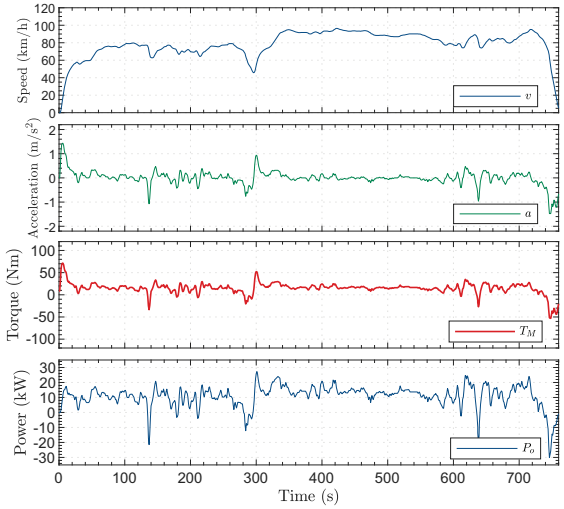

Fig. 8: HWFET mission profile: speed, acceleration, mechanical torque and power of the vehicle.

Note, that in both modes the output voltage reference is 800 V, battery current is close to 50 A and switching frequency is 200 kHz. Here, it is possible to note both the correct voltage capacitor balancing and output voltage regulation, respectively.

The second test presents the converter operation for a power transition from boost to buck mode without and with ATC at 100°C, depicted in Fig. 6 and Fig. 7, respectively. In both figures, the output power is changed by using a constant piecewise power profile, while switching frequency is fixed to 80 kHz. Note that, under boost and buck mode the pairs $\{S_2, S_3\}$ and $\{S_1, S_4\}$ present the maximum temperature, respectively. Finally, without ATC the temperature variation range is 80°C, while with ATC this range is reduced to 20°C only for one particular mode.

B. HWFET Standard Profile

In order to validate the proposed ATC strategy over a wide power operation range of the TLBBC, a MPO scenario based on Highway Fuel Economy Test (HWFET) is presented. The speed data profile has been obtained from [22]. The speed profile and the model derived in Section II-D are used to compute relevant electromechanical variables, such as acceleration, electric torque and output electric power illustrated in Fig. 8. This power is used as a reference to disturb the system with a controlled current source connected at the converter output to emulate the power delivered by the traction system. Then, with the derived electric power profile, dynamic tests focused on the ATC behaviour are performed.

The next displayed waveforms are the variables related to the converter operation such as output power/voltage/current, capacitor voltage balancing, battery current and neutral point current in Fig. 9. The output voltage is regulated at 800 V, while battery current is positive (at motoring or boost mode) and negative (at breaking or buck mode) according with the mode operation of the converter. Note that, the operation of

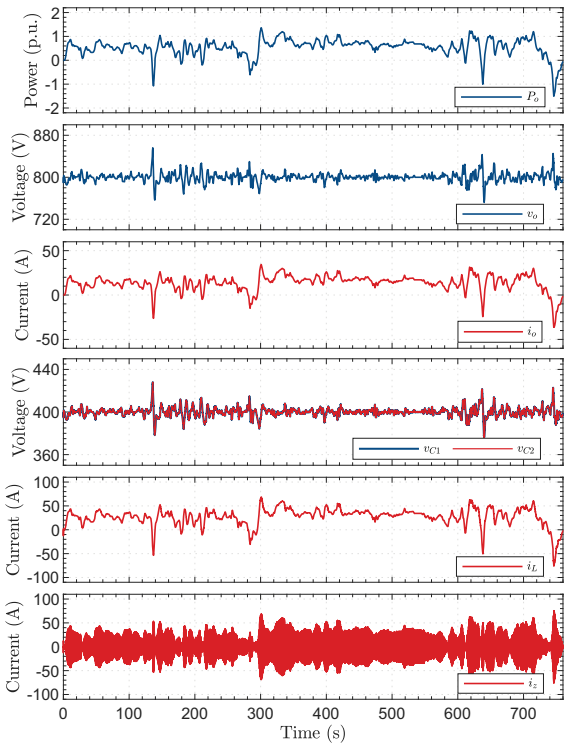

Fig. 9: Main variables: output voltage, output current, capacitor voltages, battery current and neutral point current under under HWFET mission profile.

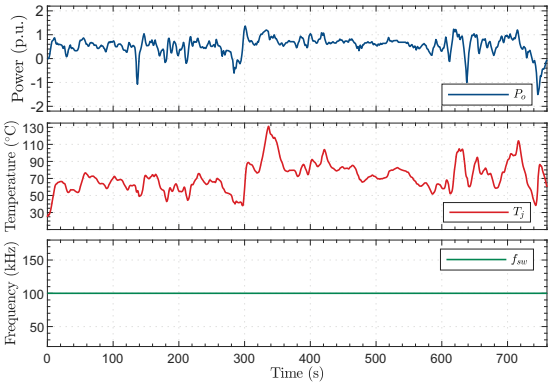

Fig. 10: Thermal dynamics: output power, estimated junction temperature and switching frequency without ATC.

the TLBBC is extended to a wide range operation conditions derived from the HWFET mission profile.

The last presented waveforms are the output power, estimated maximum junction temperature and computed switching frequency to a junction reference of 70°C. This value is selected to be related with the cooling temperature system of the overall vehicle. When the ATC is disabled and the switching frequency is fixed to 100 kHz, the obtained estimated maximum junction temperature is presented in Fig. 10. Here the temperature variation range is 90°C. On the other hand,

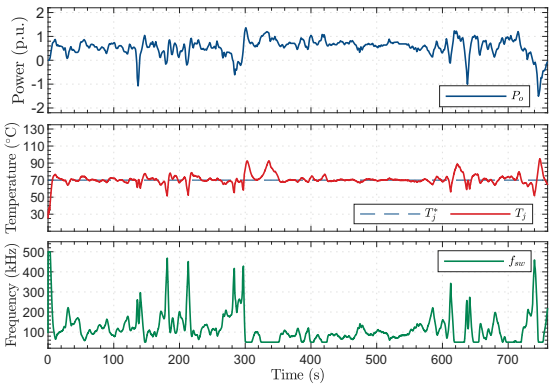

Fig. 11: Thermal dynamics: output power, estimated junction temperature and switching frequency with ATC.

when the ATC is enabled as shown in Fig. 11, the maximum junction temperature oscillates from 50 to 90°C only, i.e., the temperature variation is considerately reduced, and the thermal response is flat over the wide mission profile operation range operation. Finally, this reduction is reflected in a better thermal stress behaviour of the power converter.

V. Conclusion and Future Work

This work presents a TLBBC based on GaN HEMT semiconductor devices used as interface between a battery bank and an motor inverter. The paper presents a control scheme for junction temperature regulation, which are implemented as an active thermal control. The scheme, previously only tested for boost operation, has been successfully enhanced to include buck operation (regenerative mode). The main contribution of this paper is the development of a high-power density converter for powertrain application in EVs, which incorporates an active thermal control scheme in order to mitigate the converter thermal stress. Furthermore, the effectiveness of proposed control schemes have been verified through mission-profile-oriented simulation results. Experimental verification of the converter with the proposed complete control scheme will be developed in a future work.

Acknowledgment

This work was supported by ANID + Fondecyt Regular + 1210757, by ANID-Basal Project FB0008 and by ANID/FONDAP/15110019.

References

[1] IEA, "Global EV Outlook 2020," 2020. [Online]. Available: https://www.iea.org/reports/global-ev-outlook-2020

[2] H. Tu *et al.*, "Extreme Fast Charging of Electric Vehicles: A Technology Overview," *IEEE Trans. Transport. Electrific.*, vol. 5, no. 4, pp. 861–878, 2019.

[3] A. Khaligh and M. D'Antonio, "Global Trends in High-Power On-Board Chargers for Electric Vehicles," *IEEE Trans. Veh. Technol.*, vol. 68, no. 4, pp. 3306–3324, 2019.

[4] S. Rivera *et al.*, "Bipolar DC Power Conversion: State-of-the-Art and Emerging Technologies," *IEEE Trans. Emerg. Sel. Topics Power Electron.*, pp. 1–1, 2020.

[5] V. Monteiro *et al.*, "A Three-Level dc-dc Converter for Bipolar dc Power Grids: Analysis and Experimental Validation," in *IECON 2020 The 46th Ann. Conf. of the IEEE Ind. Electron. Soc.*, 2020, pp. 3761–3766.

[6] M. Eull and M. Preindl, "Bidirectional three-level DC-DC converters: Sum-difference modeling and control," in *2017 IEEE Transp. Electr. Conf. and Expo. (ITEC)*, 2017, pp. 573–578.

[7] D. Zhang *et al.*, "Three-Phase Bidirectional Buck-Boost Current DC-Link EV Battery Charger Featuring a Wide Output Voltage Range of 200 to 1000V," in *2020 IEEE Energy Conv. Congr. and Expo. (ECCE)*, 2020, pp. 4555–4562.

[8] G. Yang *et al.*, "A Three-level Boost-Buck Converter for the Ultracapacitor Applications," in *2019 IEEE 10th Int. Symp. on Power Electron. for Dis. Gen. Sys. (PEDG)*, 2019, pp. 700–704.

[9] Z. Zhu *et al.*, "Multi-Mode Smooth Transition Technique for Three-level Cascaded Noninverting Buck-Boost DC-DC Converter," *IEEE Trans. Power Electron.*, pp. 1–1, 2021.

[10] A. Taylor *et al.*, "Comparison of SiC MOSFET-based and GaN HEMT-based high-efficiency high-power-density 7.2 kW EV battery chargers," *IEEE Trans. Power Electron.*, vol. 11, no. 11, pp. 1849–1857, 2018.

[11] GaN Systems Inc., "GS66516B 650 V E-mode GaN transistor Datasheet," 2020. [Online]. Available: https://gansystems.com/wp-content/uploads/2020/04/GS66516B-DS-Rev-200402.pdf

[12] GaNPower International Inc., "GPIHV30DDP5L N-channel 1200V30A GaN Power HEMT in TO263-5L Package Datasheet," 2020. [Online]. Available: http://iganpower.com/wp-content/uploads/2019/09/GPIHV30DDP5L_prelim_v2.pdf

[13] J. L. Lu and D. Chen, "Paralleling GaN E-HEMTs in 10kW100kW systems," in *2017 IEEE Appl. Power Electron. Conf. Expo. (APEC)*, 2017, pp. 3049–3056.

[14] X. Jia *et al.*, "DC-link voltage control strategy of a bi-directional DC/DC converter for electric vehicles," in *2015 IEEE Energy Conv. Congr. Expo. (ECCE)*, 2015, pp. 92–99.

[15] L. Tan *et al.*, "Effective voltage balance control for three-level bidirectional dc-dc converter based electric vehicle fast charger," in *2015 IEEE 10th Conf. Ind. Electron. Appl. (ICIEA)*, 2015, pp. 357–362.

[16] M. Andresen *et al.*, "Junction Temperature Control for More Reliable Power Electronics," *IEEE Trans. Power Electron.*, vol. 33, no. 1, pp. 765–776, 2018.

[17] S. Chakraborty *et al.*, "Real-Life Mission Profile Oriented Lifetime Estimation of a SiC Interleaved Bidirectional HV DC/DC Converter for Electric Vehicle Drivetrains," *IEEE Trans. Emerg. Sel. Topics Power Electron.*, pp. 1–1, 2021.

[18] R. Hou *et al.*, "Power Loss Characterization and Modeling for GaN-Based Hard-Switching Half-Bridges Considering Dynamic on-State Resistance," *IEEE Trans. Transport. Electrific.*, vol. 6, no. 2, pp. 540–553, 2020.

[19] P. Kumar Prasobhu *et al.*, "Active Thermal Control of GaN-Based DC/DC Converter," *IEEE Trans. Ind. Appl.*, vol. 54, no. 4, pp. 3529–3540, 2018.

[20] J. Kuprat *et al.*, "research on active thermal control: Actual status and future trends," *IEEE Trans. Emerg. Sel. Topics Power Electron.*, pp. 1–1, 2021.

[21] R. Gonzalez, C. A. Rojas, and L. Callegaro, "Three-level DC-DC GaN-based Converter with Active Thermal Control for Powertrain applications in Electric Vehicles," in *2021 22nd IEEE International Conference on Industrial Technology (ICIT)*, vol. 1, 2021, pp. 502–507.

[22] EPA, "Dynamometer Drive Schedules," 2021. [Online]. Available: https://www.epa.gov/vehicle-and-fuel-emissions-testing/dynamometer-drive-schedules

[23] GaN Systems Inc., "GN002 Application Note - Thermal Design for GaNPX Packaged Devices," 2020. [Online]. Available: https://gansystems.com/wp-content/uploads/2020/08/GN002-Thermal-Design-for-GaNPX-Packaged-Devices-Rev-200804.pdf

[24] P. Skarolek and J. Lettl, "GaN Transistors Cooling Options Comparison," in *2019 International Conference on Electrical Drives Power Electronics (EDPE)*, 2019, pp. 323–326.

[25] GaN Systems Inc., "GaN Systems Plecs Device Models," 2020. [Online]. Available: https://gansystems.com/plecs-device-models/

[26] L. Callegaro *et al.*, "Control design for photovoltaic power optimizers using bootstrap circuit," *IEEE Trans. Energy Convers.*, vol. 34, no. 1, pp. 232–242, 2019.

[27] BMW, "BMW i3 Media Information," 2021. [Online]. Available: https://ev-database.org/car/1145/BMW-i3-120-Ah